THESIS

SERVO BLOWER CONTROL FOR POWERED AIR PURIFYING RESPIRATORS

Submitted by

Nicholas Adam Wagner

Department of Mechanical Engineering

In partial fulfillment of the requirements

For the Degree of Master of Science

Colorado State University

Fort Collins, Colorado

Fall 2012

Master's Committee:

Advisor: Thomas H. Bradley

John D. Williams
Peter M. Young

ABSTRACT

SERVO BLOWER CONTROL FOR POWERED AIR PURIFYING RESPIRATORS

Powered air purifying respirators (PAPRs) are a form of respiratory protection that uses a motor-coupled fan to provide filtered air to a user through a positive pressure mask. Three types of PAPR devices have been developed of which breath-responsive PAPRs are the most recent. The benefits of breath-responsive PAPRs have been identified and regulatory performance requirements have been put in place for these devices, however, no devices have been certified by any regulatory agencies. This study proposes a novel conceptual design for a breath-responsive PAPR and describes a dynamic simulation of the characteristics of this new PAPR compared to a constant flow design as exercised by a simulated breathing cycle. Additionally, this study describes a prototype of the breath-responsive concept with experimental evaluation of the prototype against regulatory requirements and conceptual design targets.

ACKNOWLEDGEMENTS

First, I would like to thank my advisor, Dr. Thomas Bradley, for his wisdom, support and the opportunity to work on challenging and exciting problems throughout my time working for him. Without his direction and advice none of this would have been possible. Thank you, also, to Dr. John Williams and Dr. Peter Young for being on my thesis committee.

Thank you to my amazing girlfriend Serah Tanno, for her constant encouragement, support, and understanding. Thanks are due to my parents for their love, support, and for constantly expecting me to work to my potential.

Next, I'd like to thank my lab partner and friend Jacob Renquist for his help and sense of humor throughout the many projects we've worked on. I want to express my appreciation to the rest of our lab group for always raising the bar and for their expectation of excellence,

The funding for this project was provided by the Department of Homeland Security under DHS/FEMA award EMW-2008-FP-02216 and the Poudre Fire Authority. .

TABLE OF CONTENTS

ABSTRACT ii
ACKNOWLEDGEMENTS iii
LIST OF TABLES vi
LIST OF FIGURES vii
LIST OF ACRONYMS ix
CHAPTER 1 INTRODUCTION 1
1.1 Constant Flow PAPRs 3
1.2 Multi-Flow PAPRs 5
1.3 Breath Responsive PAPRs 7
1.4 Purpose of Project 9
CHAPTER 2 PROTOTYPE PAPR COMPONENTS 11
2.1 Prototype PAPR Plenum Design 11
2.2 Prototype PAPR Mask Selection 12
2.3 Prototype PAPR Filter Selection 13
2.4 Prototype PAPR Blower Selection 14
2.5 Prototype PAPR Motor Controller Selection 15
2.6 Prototype PAPR Battery Pack Selection 16
2.7 Prototype PAPR Pressure Sensor Selection 17
2.8 Servo Blower Controller Design 17
2.9 Prototype PAPR Monitoring Software 18
2.10 Prototype PAPR 19
CHAPTER 3 PROTOTYPE PAPR SIMULATION 20
3.1 Sensor Gain 20
3.2 Set Point 21
3.3 Controller 21
3.4 Plant 21
3.5 Disturbance 25
3.6 System Model and Simulation 25
CHAPTER 4 CONTROLLER OPTIMIZATION 30
4.1 Design Variables 30
4.2 Design Criteria 30
4.3 Evaluation Criteria / Optimization Objectives 31
4.4 Optimization Routine 33
4.5 Pareto Optimal Design Trade Study 33
4.6 Selected Design 34
CHAPTER 5 TESTING 37
5.1 Breathing Machine 37
5.2 Breathing Machine Testing 38
5.3 Human Testing 40
CHAPTER 6 ANALYSIS 42
6.1 Battery Life 42
6.2 Filter Life 45

CHAPTER 7 CONCLUSION.....47
CHAPTER 8 Suggestions for FUTURE WORK.....49
8.1 Regenerative Blower Braking.....49
8.2 Mechanical and Other Configuration Changes.....50
8.3 Commercialization Requirements.....50
REFERENCES 51

LIST OF TABLES

Table 1: Constant flow PAPR requirements adapted from NFPA 1981 (4). 3
Table 2: Breathing Machine Tests and Observed Respiration 3
Table 3: NIOSH Breath Responsive PAPR Requirements 7
Table 4: Selected Optimal Design 34
Table 5: Optimal Constant Flow Design 35

LIST OF FIGURES

Figure 1: S.E.A Group SE400 PAPR adapted from S.E.A Group (3) 1
Figure 2: Basic PAPR System Layout 2
Figure 3: Multi-Flow PAPR System Layout 5
Figure 4: Multi-flow PAPR Hypothetical Flow Diagram 6
Figure 5: Breath Responsive PAPR System Layout 10
Figure 6: Prototype Blower Plenum adapted from Dunlap, et al. (18) 11
Figure 7: 3M Full Face piece FR-7800B adapted from 3M (19) 12
Figure 8: North CBRN 40mm Filter adapted from North Safety (20) 13
Figure 9: Filter Pressure Drop vs. Flow 13
Figure 10: Pressures in Various Locations of the S.E.A 400i PAPR 14
Figure 11: Micronel U51D2-024 Fan Curve adapted from Micronel (21) 15
Figure 12: Castle Creations Phoenix Ice Lite 50 Brushless Motor Controller adapted from Castle Creations (22) 15
Figure 13: Thunder Power RC Pro Lite MS 8000mAh 3S4P Battery adapted from Thunder Power RC (23) 16
Figure 14: Omega PX40 Pressure Sensor adapted from Omega Engineering (24) 17
Figure 15: PAPR Controller Schematic adapted from Dunlap, et al. (18) 18
Figure 16: Tower Software (left) and Datalogger Software (right) 19
Figure 17: Feedback Controlled System Block Diagram adapted from Palm (25) 20
Figure 18: PID Controller with Feed Forward Block Diagram 21
Figure 19: Zero Disturbance Test Apparatus 22
Figure 20: System Process Gain Determination 23
Figure 21: Prototype PAPR Step Response 23
Figure 22: Simulated PAPR Step Response 24
Figure 23: Simulated Breathing Disturbance 25
Figure 24: SIMULINK Block Diagram 26
Figure 25: Pressure Error Over the Breathing Cycle 27
Figure 26: Simulated Control Signal Over the Breathing Cycle 27
Figure 27: Simulated Blower Pressure Output Over the Breathing Cycle 28
Figure 28: Simulated Mask Pressure Over the Breathing Cycle 28
Figure 29: Breathing Cycle Error Simulation Output Subset 29
Figure 30: PID with Feed Forward Block Diagram 30
Figure 31: Accumulated Cycle Error Block Diagram 31
Figure 33: Pareto Optimal Frontier for Controller Design Trade Study 33
Figure 34: Optimal PID Pressure Trace Over the Breathing Cycle 35
Figure 35: Constant Flow Pressure Trace Over the Breathing Cycle 35
Figure 36: Posichek[3] SCBA Flow Tester 37
Figure 37: Breathing Machine adapted from NFPA 1981 Figure 8.1.4.9 (4) 38
Figure 38: Constant Flow PAPR Breathing Machine Test Results. Red lines indicate limits of compliance with regulatory pressure requirements 39
Figure 39: Breath Responsive PAPR Breathing Machine Test Results 40
Figure 40: Human Testing Mask Pressures, Constant Flow (left) and Breath Responsive (right) 41

Figure 41: Controller Output and Power vs. Maximum Work Rate Breathing Test 43
Figure 42: Controller Output and Power vs. Normal Work Rate Breathing Test..... 43

LIST OF ACRONYMS

BPM – Breaths Per Minute

CBRN – Chemical, Biological, Radioactive, Nuclear

CFM – Cubic Feet Per Minute

HAZMAT –Hazardous Materials

IDLH – Immediately Dangerous To Life And Health

lpm – Liters Per Minute

MPC – Model Predictive Control

MVV – Maximum voluntary ventilation

NFPA – National Fire Protection Association

NIOSH – National Institute of Safety and Health

OSHA – Occupational Safety and Health Administration

PID – Proportional, Integral, Derivative

PAPR – Powered Air Purifying Respirator

PPE – Personal Protection Equipment

SCBA – Self-Contained Breathing Apparatus

CHAPTER 1

INTRODUCTION

A powered air-purifying respirator, or PAPR, is a type of personal respiratory protection equipment commonly used by hazardous materials (HAZMAT), manufacturing, medical, and first responder personnel. Similar to a conventional respirator (or gas mask), contaminated air is pulled through high efficiency filters, matched to those contaminants, by a pump or fan and supplied to the user via a mask or hood (1). The PAPR was developed as an intermediate step between negative-pressure passive respirators and positive-pressure self-contained breathing apparatuses, or SCBAs. PAPRs are for use in locations deemed not immediately dangerous to life or health (IDLH) and are designed to provide up to 30 minutes of respiratory protection during emergencies (2). An example of a commercially available PAPR system is shown in Figure 1.

Figure 1: S.E.A Group SE400 PAPR adapted from S.E.A Group (3)

The invention of the PAPR is attributed to Richard Guy in a patent issued in 1974 (4). The patent describes a “self-contained powered air-purifying respirator helmet” with a filter for

the purpose of contaminant filtration and a blower to maintain slight positive pressure, thereby excluding outside contaminants from the user. Currently, two regulatory agencies, National Fire Protection Agency (NFPA) and National Institute of Safety and Health (NIOSH), have developed standards and certify PAPRs, and a third organization, Occupational Safety and Health Administration (OSHA), supplies regulations for their use.

Though many years have passed since the invention of the PAPR, the state of the technology hasn't changed significantly. A basic PAPR system consists of four main components: a mask, a filter, a blower, and a power source. A schematic diagram of a basic PAPR system is shown in Figure 2.

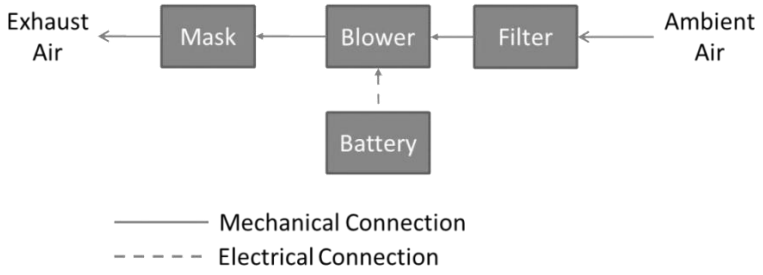

Figure 2: Basic PAPR System Layout

As the figure indicates, the battery powered blower draws air through the filter and supplies air to the mask. Different manufacturers have developed distinct strategies for meeting regulatory standards by designing, each with their advantages and disadvantages. The majority of these devices fall into two clear categories, constant flow PAPRs, and multi-flow PAPRs. A third category, breath-responsive PAPRs, corresponds to a newly developed static mask pressure and exhalation resistance requirements for which some patent literature exists, but no devices have been certified.

1.1 Constant Flow PAPRs

The majority of commercially available PAPR systems are constant flow systems. In these devices, blowers are set at a constant speed to provide proper flow to pass regulatory requirements set by NIOSH and NFPA. These requirements, summarized in the table below, must be met during a NFPA Air Flow Performance Test as described by NFPA 1981 (5).

Table 1: Constant flow PAPR requirements adapted from NFPA 1981 (5).

Requirement	**Value**
Maximum Static Mask Pressure	3.5 in. of H_2O
Zero Pressure Flow	115 lpm
Exhalation Resistance	3.5 in. of H_2O@ 85 lpm

The PAPR under test must be able to maintain mask pressure between 0 to 3.5 in. of H_2O during normal work rate and maximum work point breathing tests conducted on a breathing machine as well as be able to provide positive mask pressure while delivering 115 lpm constant flow (5). The Scott C420, for example, provides a constant 4 CFM, or 113.3 lpm at mask pressure (6). These constant flow devices are not very robust and are only designed to meet minimum regulatory breathing machine tests.

Table 2: Breathing Machine Tests and Observed Respiration (7; 8)

	NFPA Normal Work Rate	**NFPA Maximum Work Rate**	**Janssen Observed 95th Percentile 80% Workload**	**Freedman Maximum Voluntary Ventillation**
Minute Volume (lpm)	40	102	118	137.4
Breath Frequency (BPM)	24	30	30.9	31
Peak Flow (lpm)	115	300	365	432

Real users breathe differently than breathing machines, and will, in general, overtax PAPRs designed to meet regulatory requirements. Table 2 compares the characteristics of the two regulatory breathing machine tests with observed respiration from human testing performed by Janssen, et al and S. Freedman (7; 8). The maximum work rate test requires the PAPR to source 300 lpm peak, whereas Jaansen's study explains that the top 5% of men are able to exceed 300 lpm peak flow by 65 lpm (7). Additionally, the mean 4 minute sustained maximum voluntary ventillation (MVV) observed in Freedman, results in a peak flow of 432 lpm, 144% of the peak flow as specified in regulations (8).

For a PAPR that only meets the minimum 115 lpm positive pressure regulatory requirement, the user in the Freedman study would have to work against increasing filter resistance to provide the additional 132 lpm required at high workload conditions. This is a phenomenon called overbreathing (7). The pressure drop across the filters for this example can be estimated by using the same method described in Schaham, et al. (9). Pressure drop across the filter is linearly extrapolated from two points, 0 in. of H_2O at 0 lpm, and 1.968 in. of H_2O at 85 lpm. Thus, for a two parallel filter PAPR like the Scott C420, the mask pressure drop is estimated to be 1.52 in. of H_2O lower than ambient pressure at 432 lpm peak flow rate. This type of negative pressure excursion may cause contamination in some devices, however, Janssen concludes that this type of negative pressure excursion has little impact on the effectiveness of the PAPR system when matched with a negative pressure rated facepiece (7). It should be noted that NIOSH gives the same protection factor of 50 for both positive and negative pressure full faced respirators (10). OSHA, conversely, gives a protection factor of 50 to full faced air-purifying respirators, a negative pressure device, and 1,000 to full facepiece PAPRs (11).

The effects of overbreathing are not limited to contamination; overbreathing effectively increases inspiratory and expiratory resistance. That is, the breather from the example above has to work against the pressure drop in the filters to inhale, and against the back pressure provided by the exhalation valve to exhale. Many papers have been written on the physiological effects of breathing resistance. Sharkey, et al. shows a 9% decrease in work performance due to overcoming breathing resistances even smaller than the MVV example above (12). A review by Louhevaara summarizes the effects of inhalation and exhalation resistance, finding that exhalation resistance has a greater effect on work capacity than inhalation resistance, and at maximal effort the the physiological effects of respirators are significant (13).

1.2 Multi-Flow PAPRs

In order to decrease the breathing resistances found in constant flow PAPRs while still meeting the regulatory requirements, some manufacturers have developed demand-based PAPRs with three available levels of airflow. These devices measure the pressure in the mask and set the blower to one of three different flow levels based on mask pressure, which is correlatable to airflow demand. A system layout of this type of device appears below in Figure 3.

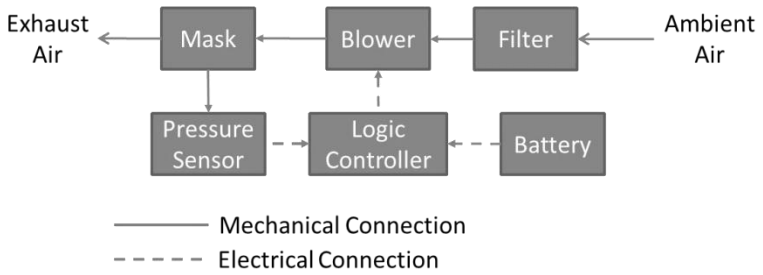

Figure 3: Multi-Flow PAPR System Layout

The layout shows the inclusion of a pressure sensor and a logic controller into the basic system layout to control the blower flowrate to one of three set points. This layout is

representative of the SEA 400i which, for example, measures the mask pressure using the pressure sensor and accelerates or retards the blower to the appropriate set point, at the end of each breathing cycle, to meet breathing demand (3).

Multiple flow levels provide two important advantages to multi-flow PAPRs: an increase in filter life, and an increase in battery life. At lower breathing levels, the multi-flow PAPR provides less than the 115 CFM constant flow that the constant flow PAPRs provide. This low blower setting causes less air to flow through the filters per unit time and requires less power from the batteries thus increasing both filter and battery life. As a result of the lower flow, exhalation resistance decreases. At higher flow rates the multi-flow PAPR will perform no differently than a constant flow system by providing a constant 115 CFM. Therefore the multi-flow PAPR results in the same breathing resistances experienced in a constant flow system. Figure 4 shows an example of this effect.

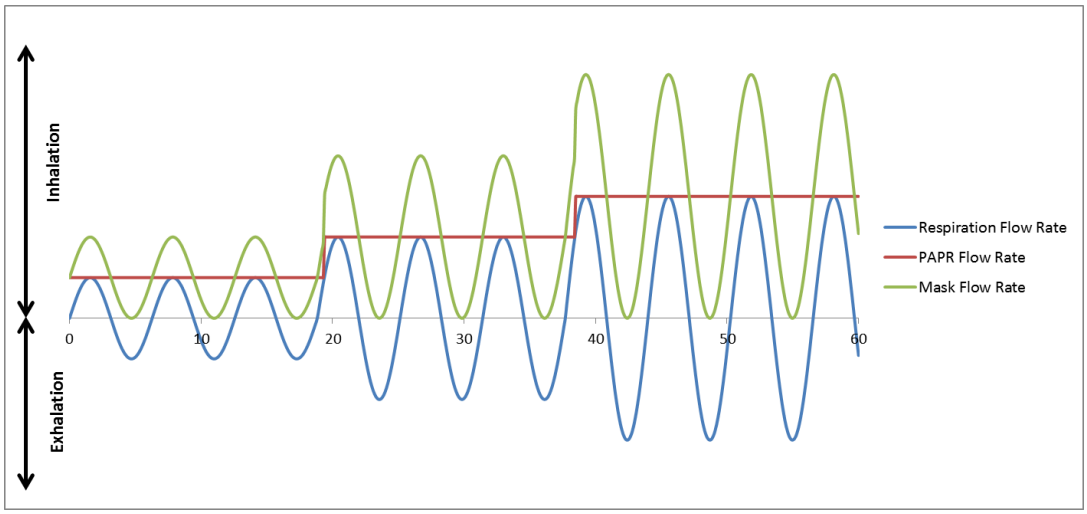

Figure 4: Multi-flow PAPR Hypothetical Flow Diagram

Figure 4 shows that in the low flow regime, the multi-flow design provides the required amount of flow to maintain positive flow from the mask (and positive pressure in the mask)

during inhalation. Because the mask pressure is approximately proportional to mask flow rate, exhalation pressure is small during low workloads. At the medium flow level, the exhalation pressure is higher, and finally, at the high flow level, the exhalation pressure is nearly identical to that of a constant flow PAPR providing a constant maximum flow.

1.3 Breath Responsive PAPRs

Another attempt at reducing inhalation and exhalation resistances, and the latest iteration on the PAPR, is the breath-responsive PAPR. These devices provide on-demand flow to the user in an effort to maintain constant positive pressure in the mask. The advantages claimed by these devices are an increase of filter and battery life, and decreased inhalation and exhalation resistances to the user. These devices claim to achieve greater filter and battery life by decreasing the throttle during times of low required flow, thus reducing the flow passing through the filter and power required of the batteries.

A new set of requirements were established by NIOSH for this new type of PAPR in 2000 and are included in Table 3, below (14). The only difference in the airflow performance requirements is a decrease of the maximum static mask pressure from 3.5 in. of H_2O to 2 in. of H_2O.

Table 3: NIOSH Breath Responsive PAPR Requirements

Requirement	**Value**
Maximum Static Mask Pressure	2 in. of H_2O
Zero Pressure Flow	115 lpm
Exhalation Resistance	2 in. of H_2O @ 85 lpm

Many patent applications for breath responsive PAPRs have been filed since 2005, three of which are described in the subsequent paragraphs. Each of the patent applications describe

different PAPR system configuration concepts to provide breath responsiveness, each with their own advantages and disadvantages.

The first patent application, US20050103343A1, describes a powered air-purifying respirator that includes a pressure sensor and an optoelectric device that reduces blower speed during exhalation and increases speed during inhalation. Blower control points are updated after each breathing cycle. A knob is provided for manual increase or decrease of flow (15). This configuration claims to provide the filter and battery life increase as well as decreased breathing resistance. Since the control system updates high and low blower speed settings once per breathing cycle, during transient breathing events, i.e. quickly transitioning from normal work rate breathing to high work rate breathing, mask pressure may go negative, causing an increase in inhalation resistance. Another notable disadvantage is that the control system would have to differentiate between inahalation and exhalation events using both the pressure sensor and the optoelectronic device. In transitions between inahalation and exhalation, the controller may lag and cause the blower to run at top speed during the onset of exhalation, thereby causing increased exhalation resistance.

Patent application US20080196723A1 describes another architecture for a breath-responsive PAPR using a control valve and blower speed controller. Pressure is measured using a transducer in the mask and a microcontroller with built-in logic uses the measured pressure to determine the correct set point for the control valve and blower speed. This PAPR provides only the flow demanded by the user. These setpoints are recalculated after each breath (16). This configuration claims filter and blower life increase as well as decreased breathing resistances, but since the controller updates only once per breathing cycle, it sufferes the same concequences as the previously described breath-responsive PAPR during transient breathing conditions.

Patent application US20100089397A1 details a third configuration for a breath-responsive PAPR with a constant speed rotory lobe blower, a pneumatically actuated valve, and a bypass conduit. Constant airflow is produced by a lobe blower to pressurize the mask. When the pressure exceeds the valve set pressure, excess air is sent back through the bypass conduit and back to the blower (17). This third configuration claims the same improvements in filter life and breathing resistances. Due to the continuous operation of the blower at top speed, the battery life advantage may not be achieved.

Two of the devices described by these patent applications have a common disadvantage in terms of a discrete and significant time delay in their dynamic response. The descriptions of these devices present update rates on the order of one breathing cycle, too slow to allow for closed loop control of pressure during a exhalation or inhalation event.

As described above, none of these designs can achieve all of the ideal characteristics of the breath-responsive PAPR concept: maintainance of constant positive pressure in the mask under dynamic breathing conditiosn, minimization of waste air to improve filter life, and minimization of wasted energy to improve battery life.

1.4 Purpose of Project

To achieve the conceptual characteristics of a breath-responsive PAPR, a servo blower control system with fast pressure feedback might be developed to provide on-demand airflow to the user to maintain a low but positive pressure in the mask. The architecture of the system appears below in Figure 5.

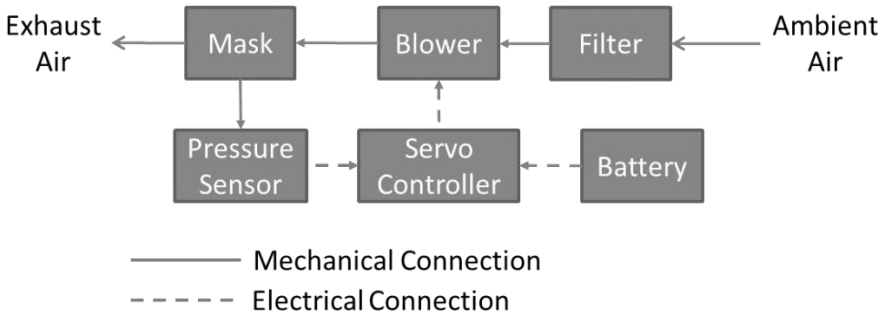

Figure 5: Breath Responsive PAPR System Layout

The servo controller is designed to maintain the pressure in the mask to some positive setpoint, by increasing blower speed following negative inhalation pressure and decreasing blower speed with positive exhalation pressure.

The purpose of this project is therefore to develop this prototype breath-responsive PAPR (Chapters 2-4), to test the prototype and a baseline constant flow PAPR against NFPA standards (Chapter 5), to provide analysis of those test results (Chapter 6), and to offer ideas for further improvements to be made to the prototype system (Chapter 8).

CHAPTER 2

PROTOTYPE PAPR COMPONENTS

This chapter discusses the design of the prototype PAPR system, specifically component selection. The following sections each focus on a single part of the PAPR system including the plenum, mask, filter, blower, motor controller, batteries, pressure sensor, and servo controller.

2.1 Prototype PAPR Plenum Design

The plenum of the prototype PAPR was developed in a 2009-2010 Colorado State University senior design project. It was designed to provide interfaces for the blower, filters, hose, and batteries and designed to meet, but was never tested nor certified to NFPA standards (18). Dimensions of the plenum can be inferred from Figure 6. Screw connections for the filters and hose are standard gasmask 40 mm DIN threads. Blower mounting holes are compatible with the product range of blowers from Micronel. More discussion on the blower can be found in section 2.4.

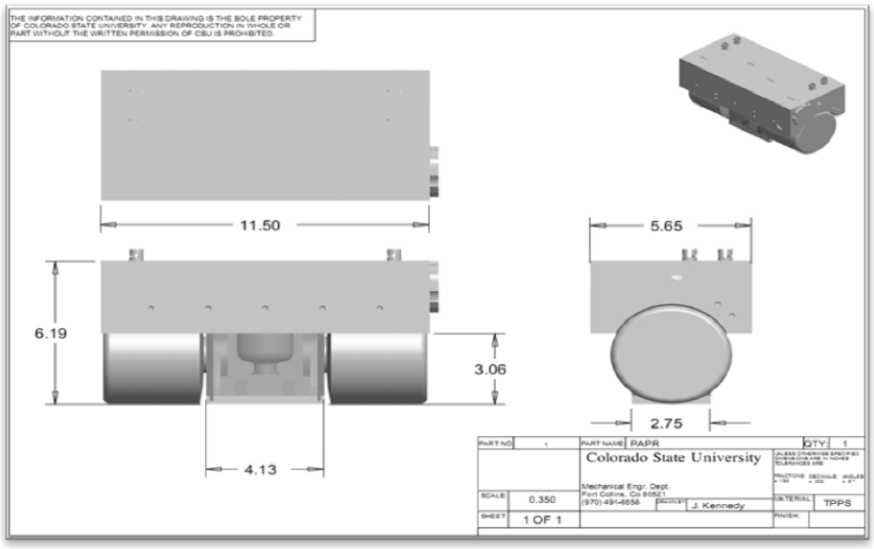

Figure 6: Prototype Blower Plenum adapted from Dunlap, et al. (18)

The prototype PAPR plenum contains extraneous geometry for mounting to an SCBA system as required by the design team, however, this geometry and the feature associated with it are not utilized in this study.

2.2 Prototype PAPR Mask Selection

OSHA and NIOSH approve the use of four different types of face pieces for powered air purifying respirators including full face pieces, half face pieces, hoods, and helmets each with their own assigned protection factor (10; 11). The mask selected by the design team is the 3M™ Full Face piece FR-7800B (18).

Figure 7: 3M Full Face piece FR-7800B adapted from 3M (19)

This mask is NIOSH-approved for use as either a negative or positive pressure application with a protection factor of 50 for NIOSH and 1000 for OSHA (10; 11). It has a low internal volume and is rigid, thus providing little pneumatic capacitance to the system, aiding in rapid transient response. The 3M mask is commercially available in small quantities at local retailers, such as Grainger. It includes 40 mm DIN connectors which are compatible with the plenum and hose connections.

2.3 Prototype PAPR Filter Selection

NIOSH certified CBRN filters are available off the shelf at any personal protection equipment retailer. For this study the North CBRN 40mm Filter Cartridge was selected. This filter is equipped with a 40 mm DIN thread consistent with other interfaces to the PAPR prototype plenum (20). The prototype PAPR plenum has interfaces for 2 filters to be installed.

Figure 8: North CBRN 40mm Filter adapted from North Safety (20)

More filters provide lower pressure drop. As previously mentioned, pressure drop over these filters can be estimated linearly using two points, 0 in. of H_2O at 0 lpm flow and 2.17 in. of H_2O at 85 lpm flow for a single filter. Providing more filters splits the flow between the filters, thus for two filters the pressure drop would be 50% that of a single filter system. The following plot illustrates the pressure drop across the filters at various flow rates.

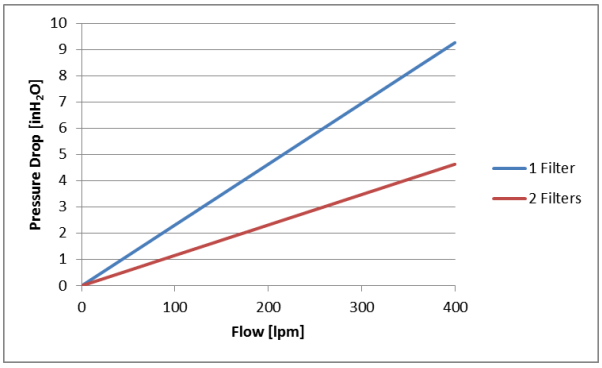

Figure 9: Filter Pressure Drop vs. Flow

For a two-filter breath responsive PAPR system, the blower will have to develop at an estimated 5 in. of H_2O at 432 lpm, the highest MVV, to overcome the pressure drop in the filters.

2.4 Prototype PAPR Blower Selection

As discussed previously, the blower overcomes system pressure drop at required flows in the system to provide necessary air to the user. These pressure drops arise from the filters, plenum, hose and exhalation valve. Using a representative system, the S.E.A 400i, pressures were measured in various locations to develop a better estimate of required pressure developed by the blower at highest flow.

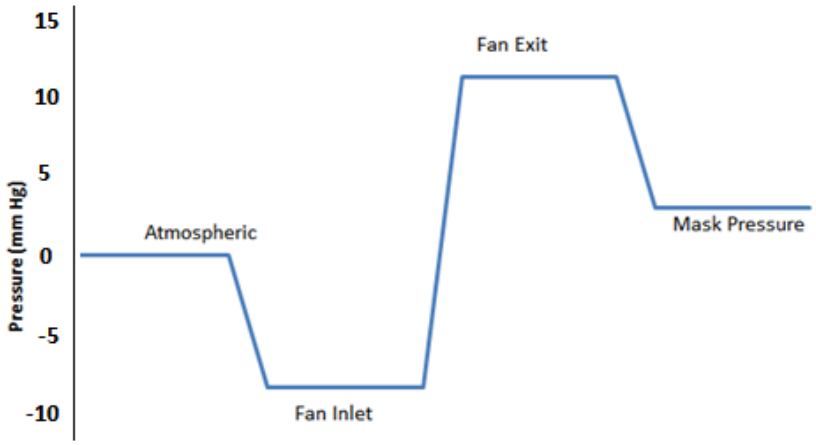

Figure 10: Pressures in Various Locations of the S.E.A 400i PAPR

As illustrated in the figure above, the blower from the S.E.A 400i develops approximately 10.7 in. of H_2O (20 mm of Hg) pressure difference from fan inlet to fan exit. The selected blower has to be able to provide this as a minimum (18).

After investigating multiple options, the Micronel U51-D2-24 was chosen to be the blower for the PAPR system (21). The pressure, volume curve for the blower is shown in Figure 11.

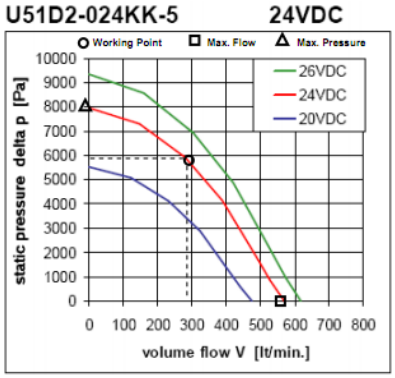

Figure 11: Micronel U51D2-024 Fan Curve adapted from Micronel (21)

Inferring from the pressure versus flow plot above, at 24V and a rate of 400 lpm the Micronel blower can create a static pressure of 10 in. of H_2O (4000 Pa) which matches the approximately 10 in. of H_2O required yet at a higher flow. This provides necessary margin to allow for over-breathing during real breathing events.

2.5 Prototype PAPR Motor Controller Selection

To electrically connect the blower to the servo controller, the system requires a motor controller. Brushless motor controllers come in many different configurations. The selected motor controller, the Castle Creations Phoenix Ice Lite 50, provides up to 50A at voltages up to 33.6V. It also provides a 5V auxiliary to power the servo controller. An image of the motor controller appears in Figure 12 (22).

Figure 12: Castle Creations Phoenix Ice Lite 50 Brushless Motor Controller adapted from Castle Creations (22)

The motor controller requires a pulsed input to control motor controller output current. This square wave input signal has a 20 ms period with a duty cycle between 5% and 10% corresponding to 0% and 100% current command respectively. This type of motor controller actuation provides a performance restriction in that the update rate will be no faster than 20 ms. Though not instantaneous, this provides vast improvement over the one breathing cycle PAPR designs currently available.

2.6 Prototype PAPR Battery Pack Selection

The battery pack was sized to provide maximum power demanded by the blower at the required voltage for 4 hours. The blower was tested to determine power at maximum throttle setting and found to be 40 Watts, thus 160 Wh was needed. At the specified 24V, the battery pack needed to be 6.66 Ah. Surveying available battery packs, two Thunder Power RC Pro Lite 8000mah 3S4P batteries were used in series to provide the necessary power and capacity.

Figure 13: Thunder Power RC Pro Lite MS 8000mAh 3S4P Battery adapted from Thunder Power RC (23)

This battery combination contains 177.6 Wh (23) which exceeded the required 160 Wh to provide maximum flow for 4.44 hours, exceeding the 4 hour requirement by 11%.

2.7 Prototype PAPR Pressure Sensor Selection

The pressure sensor, installed in the mask, needed to be able to measure both positive and negative gage pressures experienced in the mask. To meet the controller requirements, the output of the sensor needed to be an analog voltage 0-5V. The Omega PX40 pressure sensor, below, was selected because it was capable of measuring pressures between -40 to 40 mmHg (-21.4 in. of H_2O to 21.4 in. of H_2O) and providing 0-5V analog output (24). This pressure sensor was electrically connected to the controller analog input and is an integral part of the control system.

Figure 14: Omega PX40 Pressure Sensor adapted from Omega Engineering (24)

2.8 Servo Blower Controller Design

The final component to the designed system is the servo blower controller. There are two facets to the design of this controller, the hardware and the firmware. This section will focus on the hardware development; subsequent chapters are devoted to development of the firmware.

The controller interfaces both the pressure sensor and the blower motor controller requiring a digital output and an analog input which was accomplished by way of an Atmel ATMEGA 164 microcontroller. The design and manufacture of the controller board was completed by Tim Schneider, an undergraduate research assistant at Colorado State, the schematic of which appears below.

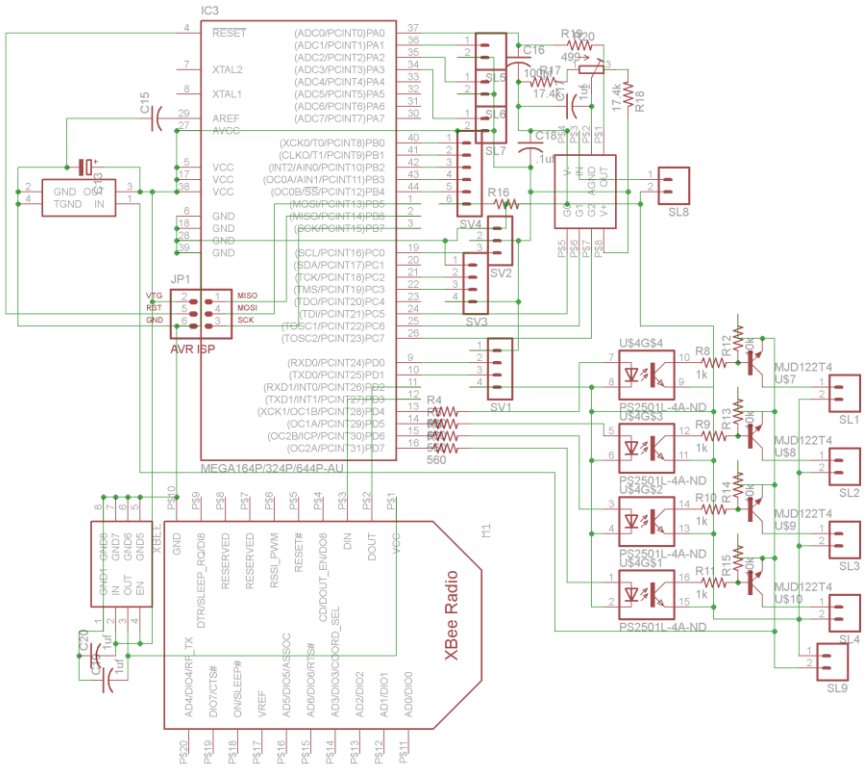

Figure 15: PAPR Controller Schematic adapted from Dunlap, et al. (18)

As designed, the controller included other features including an indicator speaker, and LEDs as well as a wireless radio which provided real time monitoring of the prototype PAPR (18).

2.9 Prototype PAPR Monitoring Software

To monitor the status of the prototype, control tower and data logger software were created. The tower software allows for real time visualization of data from the prototype

including the mask pressure, pressure error, and PWM command. This software was mainly used for troubleshooting the design.

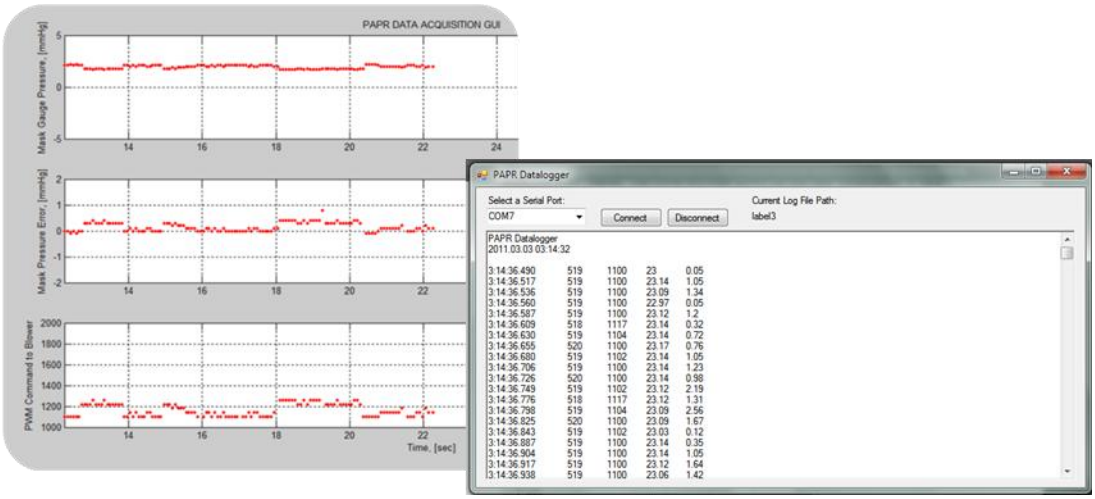

Figure 16: Tower Software (left) and Datalogger Software (right)

The data acquisition software recorded all outputs from the PAPR prototype to a text file including a time stamp, controller output, mask pressure, battery voltage, and battery current. These files were later used for the analysis presented in Chapter 6.

2.10 Prototype PAPR

Combined, these selected components compose the prototype design. By modifying the code on the microcontroller, the prototype can act as either a constant flow device or as a breath responsive device. This allows for direct comparisons of the prototype breath responsive architecture versus the constant flow architecture. The following chapters discuss the development of the prototype software.

CHAPTER 3

PROTOTYPE PAPR SIMULATION

This chapter discusses the development of the prototype PAPR simulation. The simulation of the PAPR is used in the controller optimization and is an integral part of the controller firmware design. Due to the relative simplicity of the system, it is easily modeled by the simple feedback system block diagram (25) as shown in Figure 17.

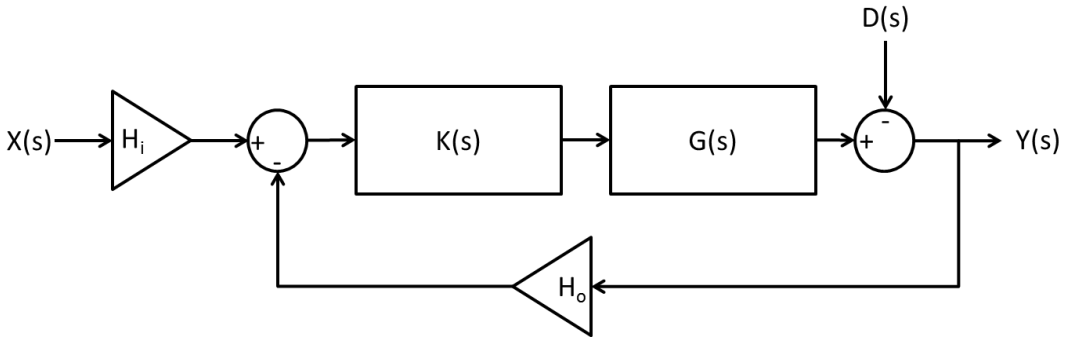

Figure 17: Feedback Controlled System Block Diagram adapted from Palm (25)

Six components make up the system model: feedback gain, H_o, controller, *K(s)*, plant, *G(s)*, and disturbance, *D(s)*. Each of these components will be discussed in further detail in subsequent sections.

3.1 Sensor Gain

The input, output, and feedback units for the system are all consistent as bits. The controller converts the analog voltage output from the pressure sensor into a 10 bit digital value from 0 to 1024 bits. Since the range of the sensor is -21.4 to 21.4 in. of H_2O, each bit corresponds to approximately 0.041 in. of H_2O. The output of the sensor at atmospheric pressure is 512 bits. To simplify the model, bits will be the consistent unit used in the simulation, thus the sensor gain is unity.

3.2 Set Point

The system set point is the desired steady state mask pressure of the system. After investigating the S.E.A 400i, a mask pressure set point of 0.5 in. of H_2O was selected. This pressure also corresponded with exhaust valve opening pressure providing constant mask airflow. Converted to bits, the system set point is 524 bits.

3.3 Controller

The servo controller developed for the prototype PAPR system was chosen to be a PID regulator with feed forward due to the dynamic nature of the system. The PID controller has the ability to quickly respond to mask pressure changes due to breathing while limiting steady state error.

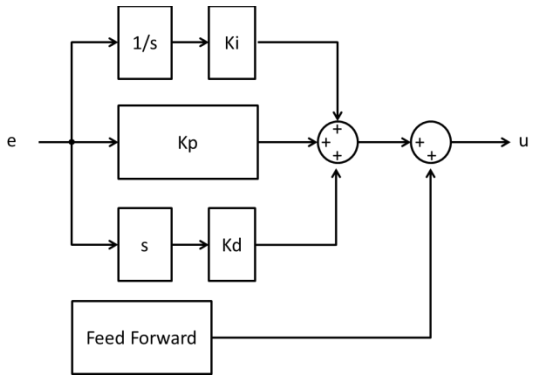

Figure 18: PID Controller with Feed Forward Block Diagram

The gains and feed forward parameters of this controller were designed through simulation in the loop optimization. This process is discussed in detail in Chapter 4. Additionally, the output of the PID controller is saturated by the motor controller at 2000 ms.

3.4 Plant

The plant consists of the filter, blower, and mask system. Since the plant exhibits low capacitance, the plant can be modeled with a first order transfer function (25).

$$G(s) = \frac{K_{ss}}{\tau s + 1}$$

A first order plant transfer function is modeled with two parameters: process gain, K_{ss}, and process time constant, τ. The validity of using a first order model and the parameters of the first order plant were experimentally determined by running two tests on the zero disturbance test apparatus shown in Figure 19, below.

Figure 19: Zero Disturbance Test Apparatus

In the zero disturbance test apparatus, the prototype PAPR system mask is connected to a mannequin head to mimic the seal on a human face without the dynamic effect of breathing. This test setup, though primitive, facilitated the completion of process gain and time constant determination testing described below.

To determine the process gain, the blower was sent command signals and corresponding steady state mask pressure was measured over the whole range of operation. The slope of the linear fit to the resulting data is a close approximation to the steady state gain.

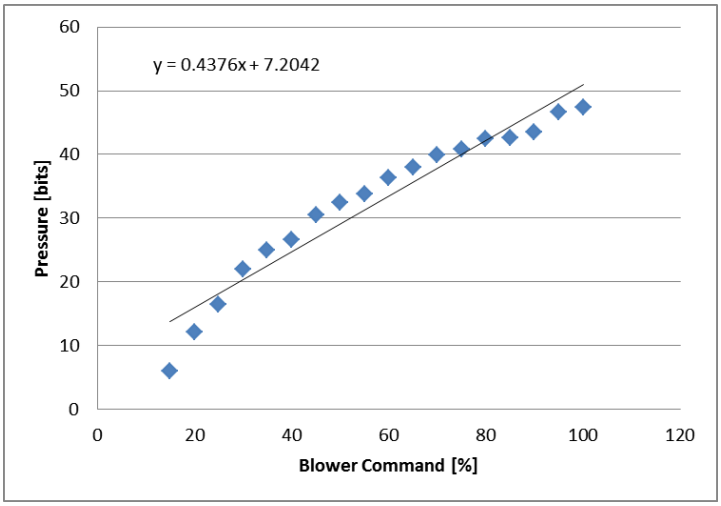

Figure 20: System Process Gain Determination

The plot above shows measured mask pressure for various controller pulses. Mask pressure is shown in bits, the digital representation of the analog voltage signal from the pressure sensor. The slope of the linear fit to the data, or the system process gain is 0.4376.

To determine the process time constant, the blower was sent a 100% command signal and pressure was measured at regular intervals until maximum pressure was reached. The duration that passes until the mask pressure reaches 63.2% of the maximum value is one time constant (25).

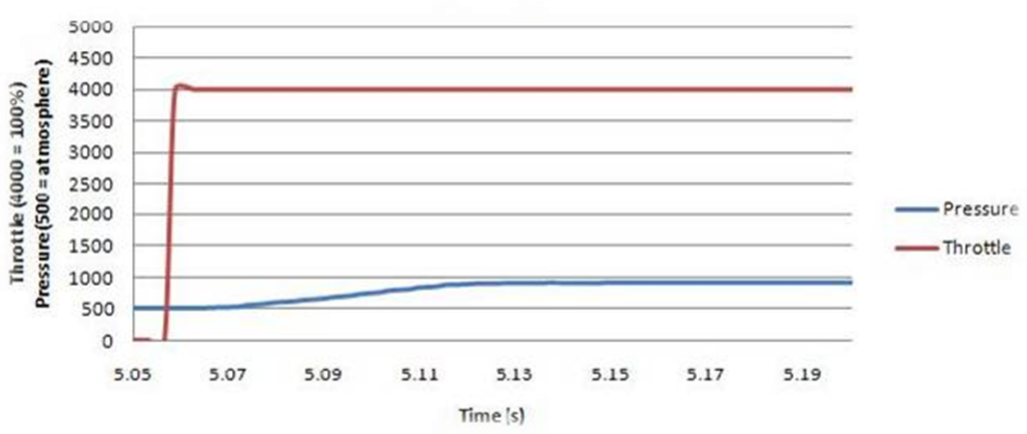

Figure 21: Prototype PAPR Step Response

For the prototype PAPR system, the total rise time is approximately 0.045 seconds with a time constant of only 0.0219 seconds, as seen in Figure 21. The results from both of these tests then define the plant transfer function.

$$G(s) = \frac{0.4376}{0.0219s + 1}$$

The step response of the experimentally determined transfer function appears in Figure 22. This response can be compared to the pressure response trace presented in Figure 21. In both cases, the simulated step response is a good approximation of the actual step response with minor differences due to two factors. The first is modeling error due to the first order system assumption. Modeling the plant as a first order system removes some of the dynamic effects of the blower, hose, and mask. Second, the speed at which the pressure needs to be measured is far greater than the sensor and controller allow. These errors are believed to be small and should have limited impact on the results of the simulation.

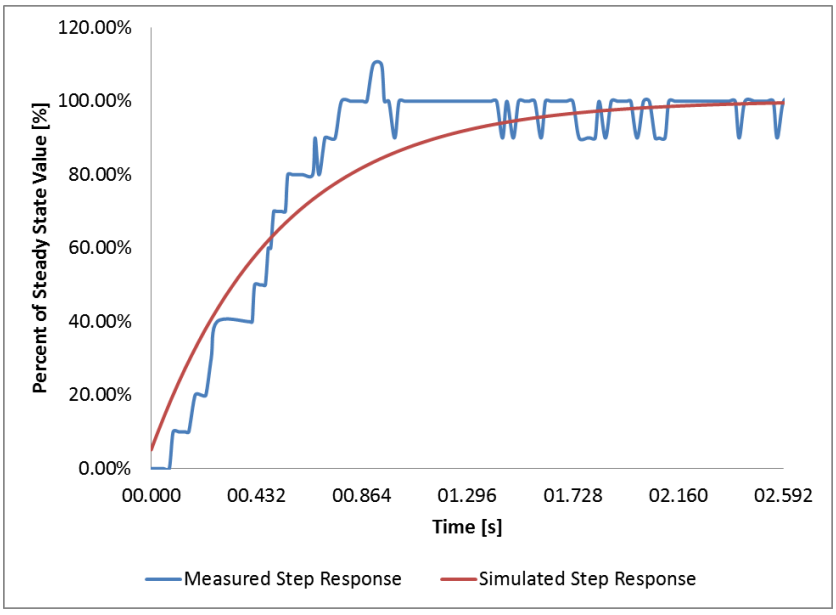

Figure 22: Simulated PAPR Step Response

3.5 Disturbance

The disturbance in the model shown in Figure 17 is the breathing of the PAPR user. Breathing is modeled as a disturbance because it disturbs the pressure regulator controller from its equilibrium condition. Since the controller will have to work in many breathing scenarios, a variable amplitude and variable frequency sinusoid is used to demonstrate disturbance rejection in simulation. The full breathing cycle model from the simulation is shown below, in Figure 23.

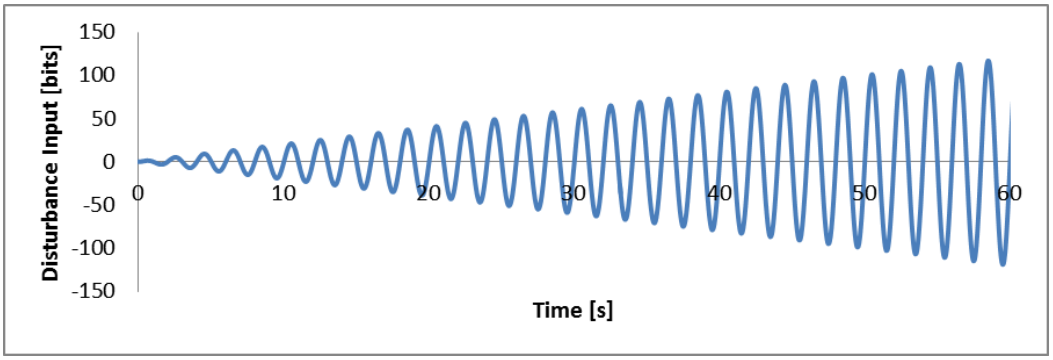

Figure 23: Simulated Breathing Disturbance

The controller gains, discussed in detail in Chapter 4, are optimized to reject disturbance, thus, the disturbance needed to incorporate different magnitudes and frequencies. The breathing model sinusoidal function, shown below, increases in both magnitude and frequency over time and was designed for this purpose.

$$f(t) = 120 * (t/60) * sin(.8\pi * t - 0.2)$$

The maximum magnitude of the disturbance function is 120 bits, or 4.9 in. of H_2O at a rate of about 30 breaths per minute.

3.6 System Model and Simulation

With a completed plant, sensor, actuator, and disturbance model, the system can then be developed in the MATLAB Simulink simulation environment, the block diagram of which

appears in Figure 24. Additional portions of the block diagram for controller evaluation have been omitted for clarity. These omitted components are described in detail in Chapter 4.

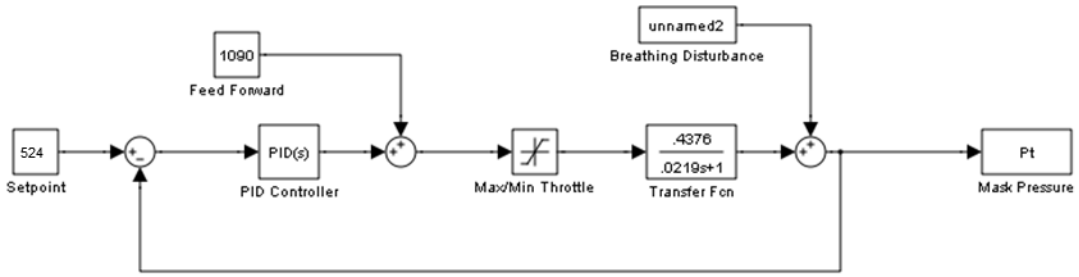

Figure 24: SIMULINK Block Diagram

Similar to the system block diagram, the SIMULINK block diagram consists of a set point, a PID controller, the plant, and the breathing disturbance. Pressure regulation error is calculated as the difference between the mask pressure and the set point pressure. This error is fed to the controller to determine a control pulse command to the plant. The output of the plant model is mask pressure. Finally, the disturbance pressure at that time point is added to the plant pressure output to determine the mask pressure. This cycle is iterated for every time point in the breathing cycle.

To run the simulation, the controller parameters need to be set. Optimization of the controller parameters used in the final design are explained in detail in Chapter 4. For the following example MATLAB auto-tuned PID parameters and feed forward were set to illustrate the execution of the model.

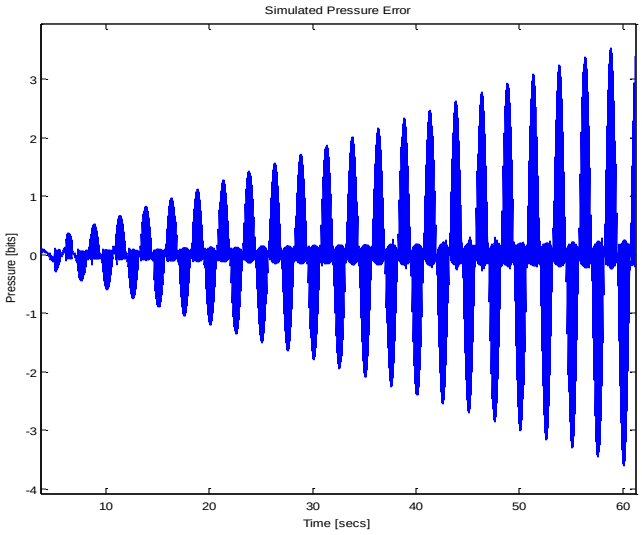

Figure 25: Pressure Error Over the Breathing Cycle

Figure 25 illustrates the set point error, or the difference between mask pressure and set point, for each time point of the breathing cycle. This error is the input to the PID controller and used to produce the blower command shown in Figure 26.

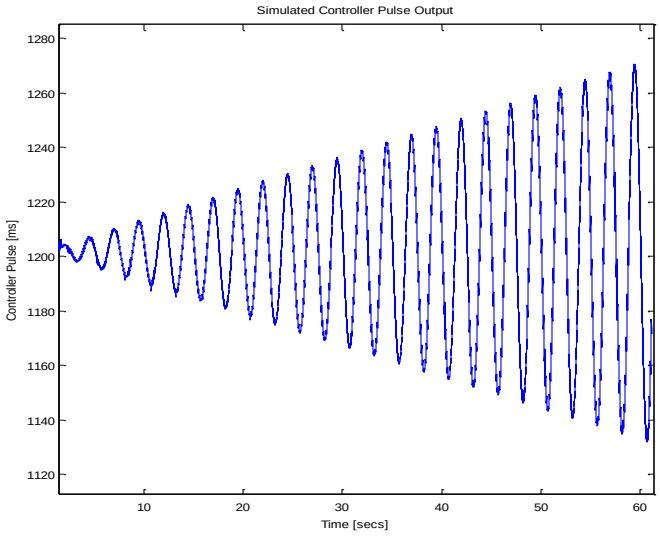

Figure 26: Simulated Control Signal Over the Breathing Cycle

As the magnitude of the pressure error increases, the blower command increases accordingly. This signal is input to the plant transfer function, which simulates the blower and motor controller to produce a simulated pressure output as shown in Figure 27.

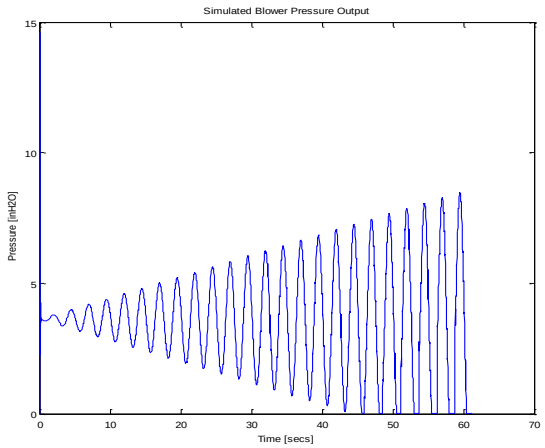

Figure 27: Simulated Blower Pressure Output Over the Breathing Cycle

The simulated blower pressure output is combined with the pressure disturbance from the breathing model to determine mask pressure, Figure 28.

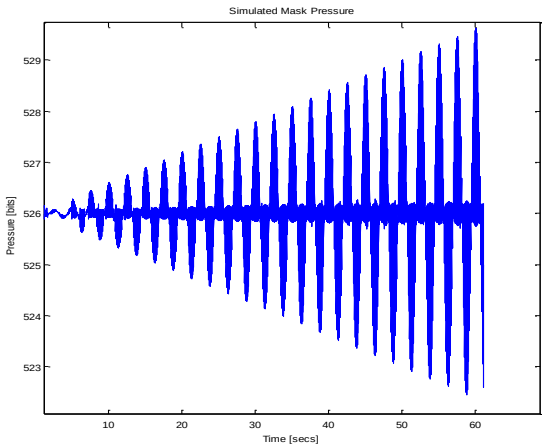

Figure 28: Simulated Mask Pressure Over the Breathing Cycle

The mask pressure is subtracted from the set point to find the error and the simulation cycles through these steps through the entire breathing cycle

In this example, there is a considerable amount of oscillation in the mask pressure. This is caused by the time delay from when the motor controller receives the pressure command to the output of the blower meeting the desired pressure.

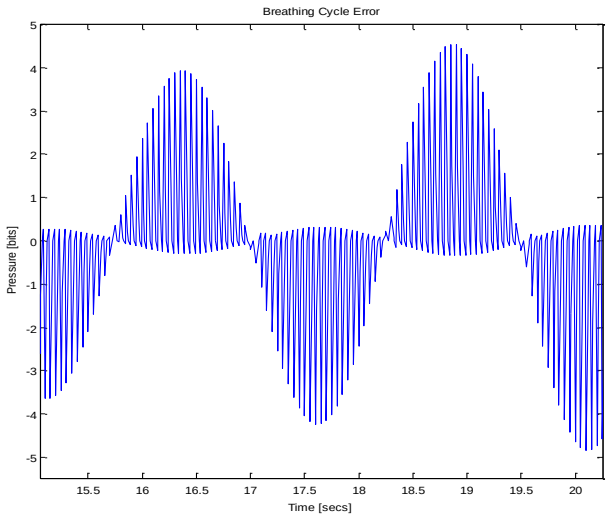

Figure 29: Breathing Cycle Error Simulation Output Subset

By zooming into a small portion of the cycle as shown in Figure 29, the pressure delay between when the pressure is demanded by the user and when the pressure is developed by the blower can easily be seen.

CHAPTER 4

CONTROLLER OPTIMIZATION

Upon completion of the PAPR simulation, the system model was incorporated into an optimization routine. The optimization routine varies the design variables to maximize/minimize evaluation criterion, subject to constraints. The following sections discuss the parameters of the optimization, a trade study of Pareto optimal designs, and preliminary simulation results.

4.1 Design Variables

The design variables optimized are the proportional gain, *Kp*, integral gain, *Ki*, derivative gain, *Kd*, and feed forward as shown in the controller block diagram presented again below. Each of the design variables is constrained to be values between 0 and 1024 as limited by the prototype PAPR controller.

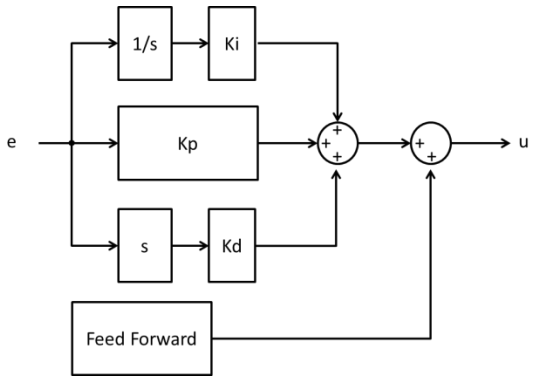

Figure 30: PID with Feed Forward Block Diagram

4.2 Design Criteria

Each design is constrained to the maximum and minimum pressures allowed by the NIOSH requirements, 0 in. of H_2O and 2 in. of H_2O (512 and 560 bits) for inhalation and

exhalation respectively. This parameter is evaluated for only the first half of the breathing cycle as the simulated disturbance exceeds blower capacity, that is, all controller designs would fail this criterion. If the design fails to meet those requirements, then it is rejected.

4.3 Evaluation Criteria / Optimization Objectives

Two different criteria are used to evaluate the designs and are used as optimization objectives. The first criterion is the integral of the absolute value of the pressure error or the accumulated absolute pressure error. This metric determines how well the controller is able to maintain the set point pressure in the mask over the breathing cycle and combines both positive and negative error. The design with the lowest accumulated absolute pressure error best tracks the breathing cycle. The block diagram used to calculate this metric is shown in Figure 31. In this calculation, the instantaneous error, the set point minus the mask pressure, is made positive and integrated over the whole breathing cycle. Units for this metric are bit-seconds. A zero bit-second accumulated cycle error means perfect breath tracking. This first criterion is designed so as to be maximized for a low-pressure error, high performance PAPR.

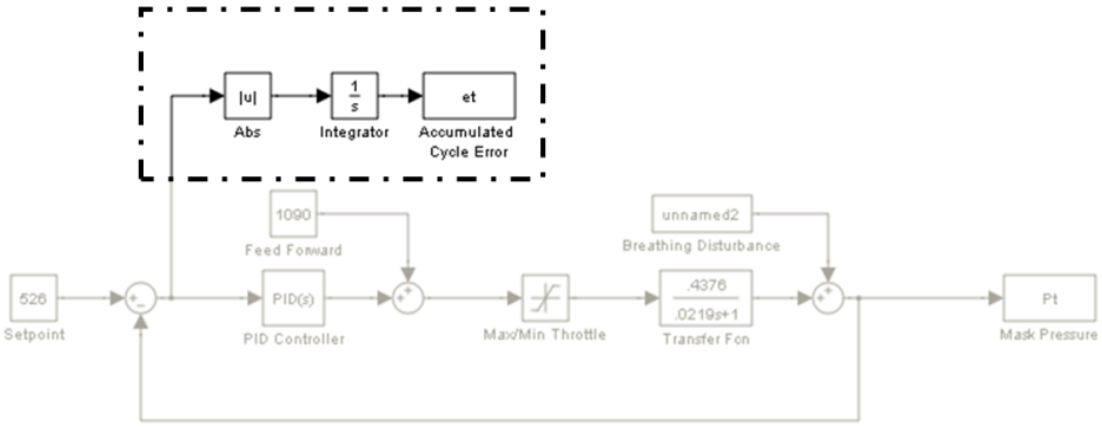

Figure 31: Accumulated Cycle Error Block Diagram

The second criterion is the controller maximum output derivative. The purpose of this criterion is to limit the rate at which the controller can change the speed of the blower. This derivative has units of bits per second. Since the output of the controller in bits corresponds to the rotational velocity of the blower, the derivative of the controller output is proportional to blower acceleration. In experimentation, it was found that the current required of the blower was strongly correlated to the acceleration of the blower. By minimizing the maximum derivative of the throttle, the power required of the battery is also minimized. The block diagram used to calculate this metric appears in Figure 32. For each time point, the controller derivative is recorded and at the end of the simulation, the maximum derivative is found. This second criterion is designed so as to be maximized for a low-power, high endurance PAPR.

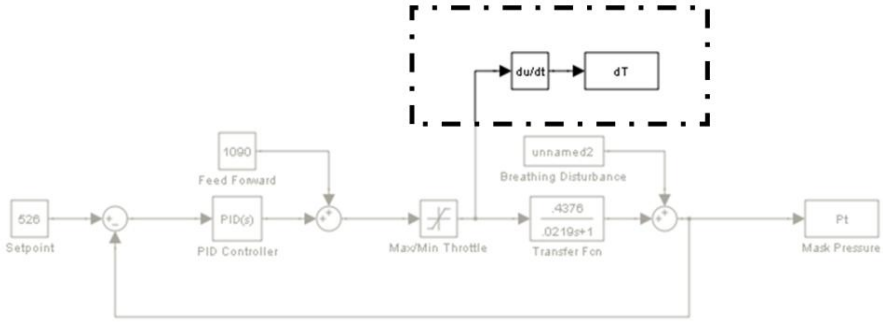

Figure 32: Maximum Controller Output Derivative Block Diagram

Having two optimization objectives requires either the use of a weighted cost function or a trade study to select an appropriate design. Defining a cost function would allow a single optimal design to be chosen, but requires predetermination of the values of the cost function weightings. Instead, so as to more fully understand the tradeoffs among these two design objectives, this study uses a trade so that many designs may be evaluated for their effectiveness

and the cost of accumulated cycle error versus the maximum controller derivative can be identified.

4.4 Optimization Routine

Darwin, a genetic algorithm (GA) developed by Advanced Design and Optimization Technologies, Inc. (Blacksburg, VA) is employed to search for optimal solutions. The key advantage to using a GA for multiple objective optimization is that GAs are capable of finding many near-optimal designs, providing many options when selecting a final controller design (26).

4.5 Pareto Optimal Design Trade Study

The result of the optimization is the trade study shown below in Figure 33.

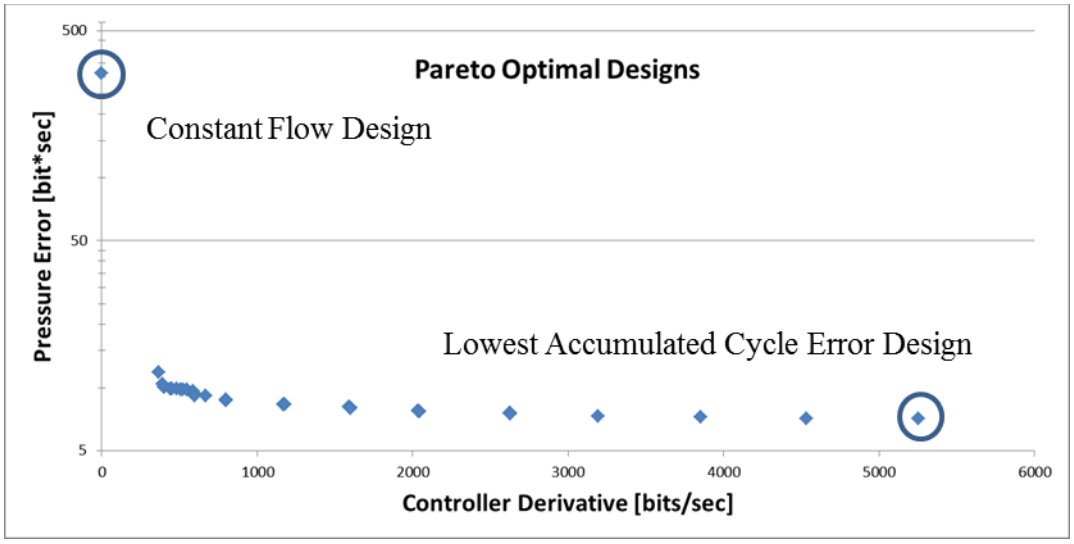

Figure 33: Pareto Optimal Frontier for Controller Design Trade Study

Each point represents an independently optimized design. As the plot indicates, designs with higher maximum control derivative have lower total error. In the same way, designs with lower maximum control derivative exhibit higher total pressure error.

One design identified by the GA optimization has a zero maximum control derivative. This design is one in which the PAPR controller commands the minimum constant flow required to meet maximum and minimum mask pressure requirements. This design is equivalent to the constant flow PAPR designs discussed in Chapter 1. As might be expected, the accumulated pressure error for this design is higher than that of the other designs. This is an indication that the PID-type control system is more effective at maintaining mask pressure during breathing cycles than a constant flow design.

4.6 Selected Design

Ultimately, the importance of the accumulated pressure error greatly outweighed the importance of the controller maximum derivative and a design was chosen with the lowest accumulated error. A summary of the design variables and design criteria appears in the table below.

Table 4: Selected Optimal Design

Kp	***Ki***	***Kd***	***FF***	**Maximum Controller Derivative [bits/sec]**	**Total Cycle Error [bit-sec]**	**Min Mask Pressure [bits]**	**Max Mask Pressure [bits]**
170	499	-159	1090	5254.4	7.12	482.4	559.0

As the table indicates, the optimized design effectively meets the breathing cycle with low accumulated error. Indicated mask pressures exceed regulatory limits, though, this is expected as the breathing cycle is much more intense than breathing machine cycles. As a comparison, the table below shows the same values for the constant flow design.

Table 5: Optimal Constant Flow Design

Kp	*Ki*	*Kd*	*FF*	Maximum Controller Derivative [bits/sec]	Total Cycle Error [bit-sec]	Min Mask Pressure [bits]	Max Mask Pressure [bits]
0	0	0	1210	0	314.27	445.3	613.3

Comparison of Table 4 and Table 5 shows that that the total cycle error and mask pressures for the constant flow design are much worse than for the PID design. For a better comparison, the figures below plot mask pressure over the breathing cycle for the optimal PID design as well as the optimal constant flow design.

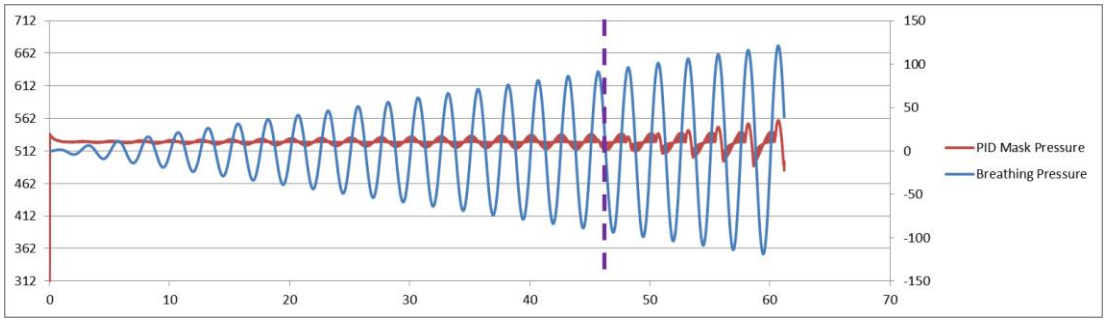

Figure 34: Optimal PID Pressure Trace Over the Breathing Cycle

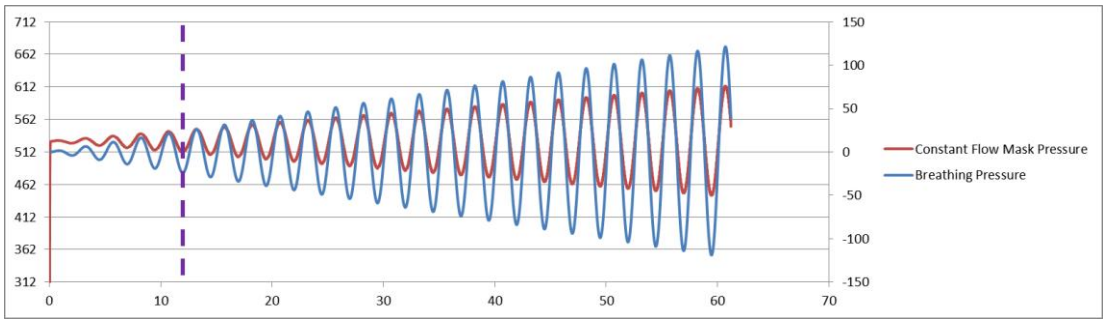

Figure 35: Constant Flow Pressure Trace Over the Breathing Cycle

For each of the designs, a vertical line is plotted to show the negative pressure crossover at which mask pressure goes below ambient and the mask would be subject to contamination.

The breathing cycle pressures at the PID design and constant flow design crossovers are -93.9 (3.8 in. of H_2O) and -23.6 bits (0.9 in. of H_2O) respectively. This difference of 2.9 in. of H_2O indicates that the PID design provides greater margin for safety at breathing pressures and rates exceeding that of the breathing machine tests.

CHAPTER 5

TESTING

This chapter discusses the testing completed to evaluate the design identified in Chapter 4. Two type of breathing tests were conducted, breathing machine, and human breathing. The first test evaluates the design to the proper requirements set by NFPA. The second test verifies the design against real breathing patterns. Breathing machine testing was provided by NIWOT Technologies, Longmont, CO.

5.1 Breathing Machine

All breathing machine testing was conducted on a Sperian Biosystems Posichek^3 SCBA Flow Tester, shown in Figure 36.

Figure 36: Posichek^3 SCBA Flow Tester

The Posichek^3 is the industry standard tool for measuring in-mask pressures of respiratory devices (27). Two flow rate tests are availible which correspond with NFPA standard and

maximum work rates. Posichek[3] uses a cam mechanism to actuate a bellows to produce a percise breathing waveform consistent with NFPA 1981.

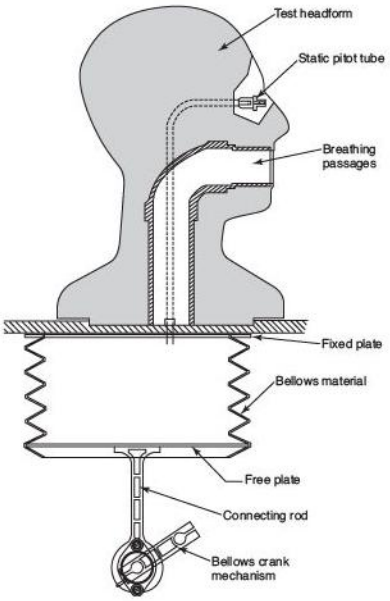

Figure 37: Breathing Machine adapted from NFPA 1981 Figure 8.1.4.9 (5)

To conduct the breathing test, the mask is attached to the test headform, the PAPR is turned on and the breathing test is initiated via computer. Each revolution of the bellows crank mechanism corresponds to one breathing cycle with one inhalation and one exhalation. The static pitot tube measures the mask pressure over the cycle and is recorded on pressure plots. Airflow is measured by the product of the breathing rate and the tidal bellows volume.

5.2 Breathing Machine Testing

In order to perform an idealback to back comparison of the two controller configurations, the controller for the PAPR was tested in both constant flow and breath responsive modes. The first mode tested is the constant flow mode. The controller is set to a constant blower throttle of 1210 bits, the optimal constant flow design as identified by the optimization. This test is the

baseline test configuration and is the basis for comparison. The second mode of operation is the optimal PID mode, the design and selection of which was described in Chapter 4.

This constant flow PAPR design was tested at both of the work rate tests in NFPA 1981, the standard work rate and maximum work rate. As explained before the standard work rate test is a 40 lpm test, and the maximum work rate test is 102 lpm. The following figure is the Posichek[3] mask pressure output from these tests of the baseline configuration.

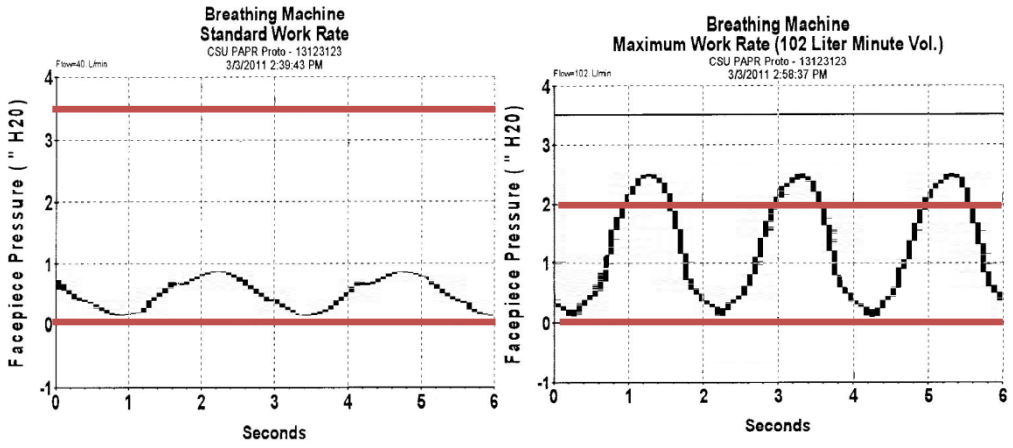

Figure 38: Constant Flow PAPR Breathing Machine Test Results. Red lines indicate limits of compliance with breath responsive PAPR regulatory pressure requirements

As can be seen in Figure 38, the constant flow PAPR meets the maximum and minimum pressure requirements for constant flow PAPRs, 0 and 3. in. of H_2O respectively, but exceeds the maximum pressure requirement for breath responsive PAPRs of 2.0 in. of H_2O. For the standard work rate, the constant flow PAPR design mask pressures modulated between approximately 0 and 1 in. of H_2O. For the maximum work rate, the pressures modulated between approximately 0 and 2.5 in. of H_2O.

The same tests were then performed on the optimal PID design. The figure below shows the Posichek[3] mask pressure plots over the breathing cycle for this design.

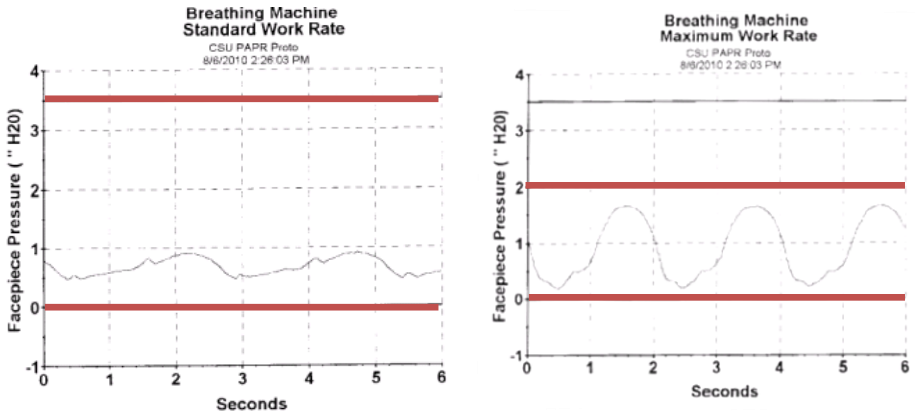

Figure 39: Breath Responsive PAPR Breathing Machine Test Results

As can be seen in the figure above, the breath responsive PAPR meets the 0 in. of H_2O minimum and maximum pressure requirements for both constant flow PAPRs and breath responsive PAPRs. 3.5 and 2 in. of H_2O respectively. For the standard work rate, the breath responsive PAPR design mask pressures modulated between approximately 0.5 and 1 in. of H_2O, which equates to a 0.5 in. of H_2O reduction in mask pressure variation compared to the constant flow PAPR. For the maximum work rate, the pressures modulated between approximately 0 and 1.5 in. of H_2O, resulting in a 1 in. of H_2O reduction in the mask pressure range compared to the constant flow PAPR.

5.3 Human Testing

Human testing was performed by Jacob Renquist, a CSU graduate research assistant, on a treadmill. Treadmill speed was increased until negative pressure excursions were experienced on the baseline constant flow design and mask pressure was recorded. The PAPR was switched over to the optimal breath responsive design and mask pressure was recorded.

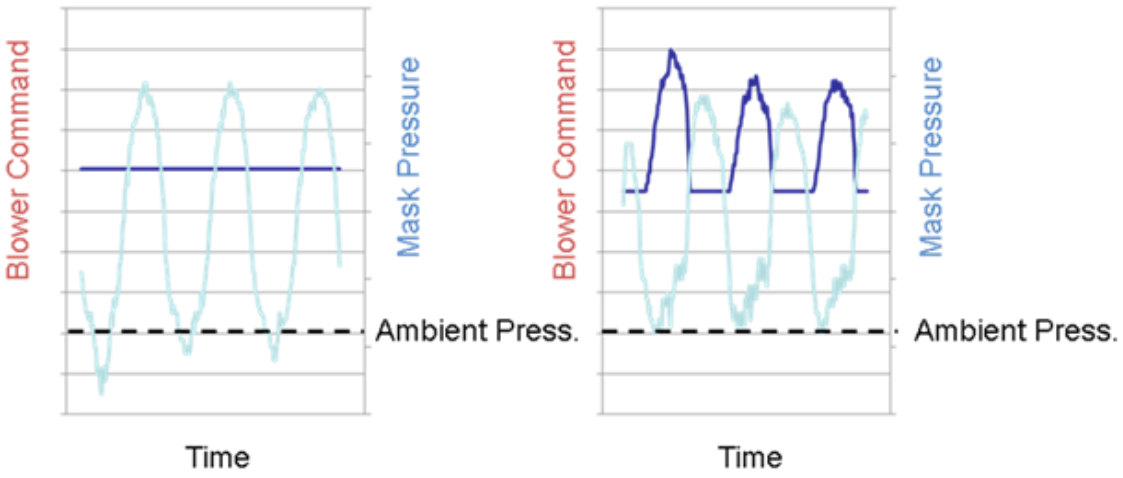

Figure 40: Human Testing Mask Pressures, Constant Flow (left) and Breath Responsive (right)

As Figure 40 shows, the breath responsive PAPR was able to meet the actual breathing cycle during exercise which exceeded the capability of the constant flow PAPR.

CHAPTER 6

ANALYSIS

The previous chapter discussed the performed testing and showed the PID PAPR design was capable of meeting the breath responsive PAPR mask pressure requirements discussed in Chapter 1. This chapter discusses the other expected advantages of the prototype breath responsive PAPR including increased battery and filter life.

6.1 Battery Life

The battery life was tested using the breathing machine at the two work rates shown in the previous chapter. Voltage and current were recorded for both designs during the tests using a resistor network and a current transducer. Measurements were taken approximately every 0.02 seconds and integrated over 10 seconds to determine the power required at the work point. The total battery life is calculated using the equation below.

$$Time = \frac{Battery\ Capacity}{Voltage * Current}$$

Figure 41displays current and torque command over 10 seconds for both designs for the high work rate test. It is clear from the figure that the power required for PID is greater than is required for the constant power throttle.

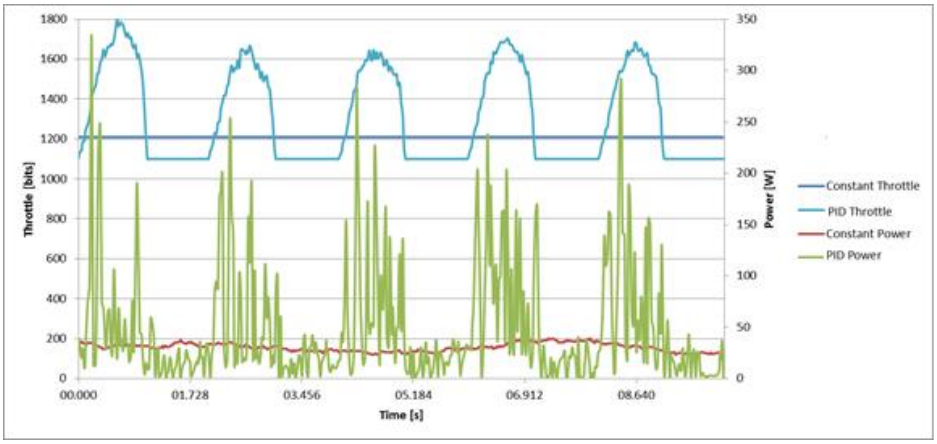

Figure 41: Controller Output and Power vs. Maximum Work Rate Breathing Test

Averaged over the 10 second cycle, the constant throttle and PID design required 30.4W and 33.4W respectively. The battery in the prototype PAPR batteries have a capacity of 177.6 Wh giving the constant throttle and PID designs theoretical battery lives of 5.8 hours and 5.3 hours respectively. At a constant high work point, the penalty of being breath responsive is only 0.5 hours for the breath responsive PAPR, a decrease of 8.6%. Similar results were found for the low work point, shown in the figure, below.

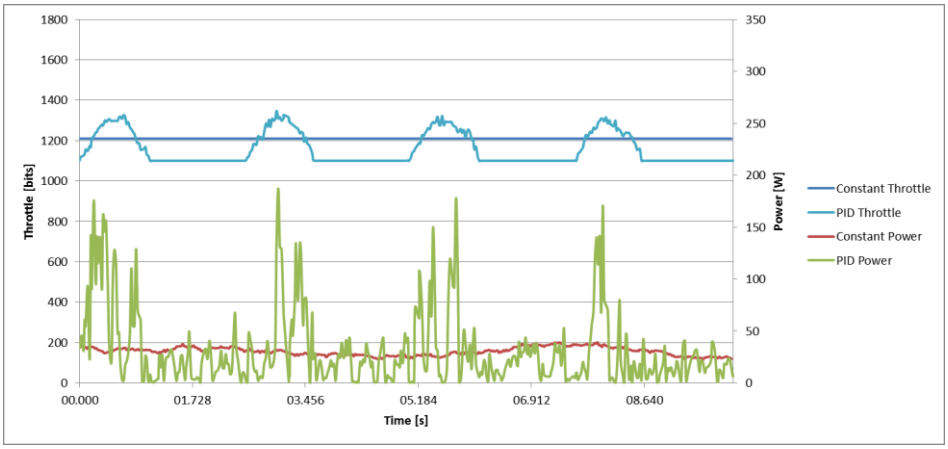

Figure 42: Controller Output and Power vs. Normal Work Rate Breathing Test

Over the 10 second cycle, the constant throttle and PID design required 30.4W and 31.0W respectively. With the prototype PAPR battery, the constant throttle and PID designs have theoretical battery lives of 5.8 hours and 5.7 hours respectively. At a constant normal work point, the penalty of being breath responsive is only .1 hours, a 1.7% reduction.

This observation was not expected, however, there are a few possible explanations. First, the power requirements of accelerating the blower can be characterized by first principals using the equation, below.

$$P = T\omega$$

At steady state, power, *P*, is the product of required torque *T*, and rotational velocity, ω. A constant speed blower could be modeled using only this equation. Assuming perfect conversion efficiency, the power required of the batteries would equal the product of the torque and rotational velocity. The required torque is caused by friction and the load on the motor from the steady state pressure and flow requirements of the PAPR.

Accelerating the blower, however, requires more torque. To accelerate the blower at the desired rate, α, the torque required is the sum of the steady state torque, above, and the product of the angular acceleration and the polar moment of inertia, *J*. Thus the power required of the motor, again assuming ideal conversion efficiency, is shown below.

$$P = (T_0 + J\alpha) * \omega$$

Decelerating the blower requires less than the steady state torque which reduces this effect, though clearly for the prototype PAPR, the periods of deceleration do not counteract the periods of acceleration.

The purpose of the multi-objective optimization discussed in Chapter 5 was to find a balance between controller derivative and cycle error. This result may be an indication that a lower controller derivative may provide battery life improvement, but as the trade study indicated, decreased controller derivative comes at a cost of accumulated cycle error.

Another possible contributor to the increase in required power is cogging. The apparent noise in the power trace for the blower is evidence of an effect where imperfections in the rotor and stator cause the rotor to either lead or lag the stator causing a speed ripple and current spikes (28). To minimize the effects of cogging, a Hall-effect sensored motor controller can be used. This is discussed in more detail in Chapter 8.

6.2 Filter Life

Filter life advantage can also be inferred from the data collected in testing and displayed in Figure 41 and Figure 42. Since a flow meter was not fitted to the PAPR system, only the throttle and mask pressure can be used to estimate the effect on filter life. Chapter 3 showed the relationship between throttle and mask pressure was fairly linear and using the relationship between flow and pressure (25), below. This study assumes that flow is also linear with torque command.

$$p = q * R_L$$

From the high work point results, the average torque command for the constant flow and PID designs are 1210 and 1304 bits respectively. This result makes intuitive sense. To increase the pressure during a high level of inhalation, higher flow is required. For a constant high work point cycle, the PID requires 7.8% more flow.

The normal work point results, however, show that the PID reduces the average throttle from 1210 to 1156. Therefore at the normal work rate, the PID design provides a 4.4% improvement in filter life.

Though the prototype PAPR was able to meet mask pressure requirements, the prototype PAPR was not able to effectively realize the expected advantages of filter and battery life due to competing design requirements, controller design selection, and hardware selection. Chapter 8 proposes changes to the prototype PAPR system that may be able to actualize these advantages.

CHAPTER 7

CONCLUSION

Over the course of the development of the PAPR, three different families of PAPR devices have been developed to improve user experience. Many studies have been conducted to determine the effects of respiratory devices on their users and indicate a decrease in performance due to physiological and psychological effects. Breath responsive PAPRs attempt to decrease these effects by minimizing breathing resistances. Of this category, three patent applications presented different ways of meeting regulatory requirements. This study also presented its own concept design using a PID algorithm to servo-control a blower using pressure feedback.

By applying this concept to a prototype PAPR device developed at CSU, the effectiveness of this concept could be evaluated. Investigating this hardware, a simulation was created for the purpose of optimizing PID controller gains to meet a simulated breathing cycle. In simulation, the optimal PID design was shown to exceed the cycle capability of the constant flow device by 2.9 in. of H_2O. In addition, inhalation and exhalation resistances during conditions much more intense than standard breathing cycles were shown to decrease by 1.52 and 2.53 in. of H_2O, respectively. Standard breathing machine testing and human testing were used to verify these results and displayed inhalation resistance decreases of 0.5 and 0 in. of H_2O and exhalation resistance decreases of .5 and 1 in. of H_2O for the normal and maximum work points, respectively.

An analysis of the effect on battery life and filter life was presented. Results indicate the prototype PAPR decreased battery life by 0.1 and 0.5 hours for the normal and maximum work point respectively, and increased filter life by 7.8% for the normal work point and decreased it by

4.4% for the maximum work point. Though the prototype PAPR was unable to realize gains in filter and battery life that were expected of this category of device, this study offers a proof of concept that a optimization of the design and control of the PAPR can describe the limits of compromise among the dueling objectives of safety, filter life and battery life. Though the prototype PAPR showed that PID control of mask pressure is a means for improvement of the safety and filter life of PAPRs, further work will need to be conducted to realize additional gains in battery life.

CHAPTER 8

SUGGESTIONS FOR FUTURE WORK

This project is a proof of concept that controllers are useful in modulating airflow of powered air purifying respirators and opens the door to many extensions to this work. This chapter discusses possibilities for expanding upon the work that has already been completed.

8.1 Regenerative Blower Braking

One of the obvious downfalls of the current configuration is the lack of active braking of the blower. The motor controller used in this research lacks the features necessary for such control. This active braking would decrease the flow and pressures developed by the blower during exhalation by decreasing the blower speed more rapidly. Using a more advanced motor controller would provide this active braking as well as other features such as regenerative braking, i.e. reclaiming power in braking. Regenerative braking provides both the advantage of improved exhalation resistance as well as improved battery life. This could provide significant improvement over the current design.

Regenerative breaking could also be achieved with a kinetic energy storage system. The blower could be clutched to a mass and energy could be transferred back and forth through the breathing cycle to assist the motor on the blower and decrease the dependence on the electrical energy. This would accrue mechanical losses instead of mechanical and electrical. Additionally, these advanced motor controllers have sensors for rotor position which would decrease the cogging effect exhibited by the controller used.

8.2 Mechanical and Other Configuration Changes

Other mechanical devices could be investigated for assisting the system like an inflatable plenum, one way valve in the hose, and flow meters.

Higher complexity controllers can be investigated for their effectiveness such as model predictive control, or MPC. Implementing MPC would allow for on the fly optimization of controller set points and parameters tailored specifically for the user and improve tracking by predicting the breathing cycle. This would be advantageous over the current PID control because it would be optimized specifically for the breathing cycle parameters experienced, not the breathing cycle used in the controller optimization.

8.3 Commercialization Requirements

Productionising a breath responsive PAPR would require further investigation into the component configuration. Since the weight of the device is critical, design of the plenum is incredibly important. Selection and design of components like the blower, filter, hose, pressure sensor, and mask selection are also important.

REFERENCES

1. **Minnesota Department of Health.** Powered Air Purifying Respirator (PAPR). *Minnesota Department of Health.* [Online] March 11, 2011. [Cited: 8 2, 2012.] http://www.health.state.mn.us/divs/idepc/dtopics/infectioncontrol/ppe/comp/papr.html#filters.

2. **Centers for Disease Control and Prevention.** Documentation for Immediately Dangerous To Life or Health Concentrations (IDLHs). *NIOSH Publications and Products.* [Online] [Cited: August 2, 2012.] http://www.cdc.gov/niosh/idlh/idlhintr.html.

3. **The S.E.A. Group.** SE400 fan units. *The S.E.A. Group.* [Online] September 25, 2011. [Cited: August 2, 2012.] http://www.sea.com.au/html/pdf/datasheet/ds_se400at-2.pdf.

4. **Guy, Richard.** *Powered Air-Purifying Respirator Helmet. 3,822,698* United States of America, January 22, 1973. Utility.

5. **National Fire Protection Agency, inc.** *NFPA 1981: Standard On Open-Circuit Self-Contained Breathing Apparatus (SCBA) For Emergency Services.* Quincy, Ma : National Fire Protection Agency, inc., 2007.

6. **Scott Safety.** C420 PLUS PAPR. *Scott Safety.* [Online] May 20, 2008. [Cited: August 2, 2012.] https://www.scottsafety.com/en/us/DocumentandMedia1/Marketing/ProductLiteratureandCatalogs/Brochures/Bro_C420Plus_HS_6716_408.pdf.

7. *Interpretation of Inhalation Airflow Measurements for Respirator Design and Testing.* **L.L. Janssen, et al.** 2005, Journal of the International Society for Respiratory Protection, Vol. 22, pp. 122-139.

8. *Sustained maximum voluntary ventilation.* **Freedman, S.** 2, January 1970, Respiration Physiology, Vol. 8, pp. 230-244.

9. **Schaham, Elhanan and Reshef, Yaron.** *Comments on Breathing Performance.* Israel : Testa Technologies, 2004.

10. **Centers for Disease Control and Prevention.** NIOSH Respirator Selection Logic. *Department of Health and Human Services.* [Online] 2004. [Cited: August 2, 2012.] http://www.cdc.gov/niosh/docs/2005-100/pdfs/05-100.pdf.

11. **United States Department of Labor.** Assigned Protection Factors for the Revised Respiratory Protection Standard. *Occupational Safety & Health Administraton.* [Online] 2009. [Cited: August 2, 8.] http://www.osha.gov/Publications/3352-APF-respirators.html.

12. **Sharkey, Brian and Gaskill, Steven.** Respiration, Respirators and Work Capacity. *3M JobHealth.* 2001, Vol. 19, 2.

13. *Cardiorespiratory effects of respiratory protective devices during exercise in well-trained men.* **Louhevaara, Veikko, et al., et al.** 52, Helsinki, Finland : Springer-Verlag, 1983, European Journal of Applied Physiology and Occupational Physiology, Vol. 1984, pp. 340-345.

14. **Centers for Disease Control and Prevention.** Breath Responsive Powered Air-Purifying Respirators (PAPRs); Notice of Acceptance and Evaluation. *Department of Health and Human Services.* [Online] April 7, 2000. [Cited: August 2, 2012.] http://www.gpo.gov/fdsys/pkg/FR-2000-04-07/html/00-8371.htm.

15. **Gosweiler, Otto.** *Breath Responsive Filter Blower Respirator System. 20050103343* United States of America, May 19, 2005. Invention.

16. **Tilley, Greg Allan.** *Breath Responsive Powered Air-Purifying Respirator. 20080196723A1* United States of America, August 21, 2008. Utility.

17. **Klockseth, Martinus O.** *Breath Responsive Powered Air Purifying Respirator Apparatus. US20100089397A1* United States of America, April 15, 2010. Utility.

18. **Dunlap, Nichole, et al., et al.** *SCAMP Final Report.* Fort Collins, CO : s.n., 2010.

19. **3M.** Full Facepiece FR-7800B with Canister FR-15-CBRN and CP3N. *3M.* [Online] June 1, 2005. [Cited: August 3, 2012.] http://multimedia.3m.com/mws/mediawebserver?mwsId=66666UF6EVsSyXTtMXM2OxTVEVtQEVs6EVs6EVs6E666666--&fn=FOD_9020.pdf.

20. **North Safety.** Product Data Sheet Information - North 54500 Series Gask Mask. *North Safety.* [Online] November 22, 2005. [Cited: August 3, 2012.] http://www.google.com/url?sa=t&rct=j&q=&esrc=s&source=web&cd=1&ved=0CGMQFjAA&url=http%3A%2F%2Fwww.northsafety.com%2FDocumentConsoleDownload.aspx%3FDC_ID%3D10029&ei=hmwcUPKIOoPG6wGorYCwDw&usg=AFQjCNHAyATXwpXvLA7IpuFDnoA36AbvUw&sig2=NXSP37q1o3TwUy6H-1iItA.

21. **Micronel.** Miniature Radial Blower. *Micronel.* [Online] October 30, 2007. [Cited: August 3, 2012.] http://www.micronel.com/proddb/datasheet_300.pdf.

22. **Castle Creations.** Phoenix Ice Brushless Motor Controls. *Castle Creations.* [Online] 2012. [Cited: August 3, 2012.] http://www.castlecreations.com/products/phoenix_ice.html.

23. **Thunder Power RC.** Thunder Power RC ProLite Series . *Thunder Power RC.* [Online] [Cited: August 3, 2012.] http://www.thunderpowerrc.com/html/prolites.html.

24. **Omega Engineering, Inc.** Miniature Voltage Output Pressure Sensors . *Omega Engineering, Inc.* [Online] [Cited: August 3, 2012.] http://www.omega.com/pptst/px40.html.

25. **Palm III, William, J.** *Modeling, Analysis, and Control of Dynamic Systems.* New York : Wiley, 2000.

26. *Powertrain Design for Hand-Launchable Long Endurance Unmanned.* **Wagner, N., Boland, S., Taylor, B., Keen, D., Nelson, J., Bradley, T.** Nashville, TN : AIAA, 2010. AIAA-2010-6689.

27. **Sperian.** Biosystems Posichek3. *Sperian.* [Online] September 2, 2008. [Cited: August 9, 2012.] http://www.honeywellsafety.com/Supplementary/Documents_and_Downloads/Instrumentation/SCBA_Test_Bench/19955/1033.aspx.

28. **Wikipedia.** Cogging Torque. *Wikipedia.* [Online] December 21, 2011. [Cited: August 9, 2012.] http://en.wikipedia.org/wiki/Cogging_torque.

29. **NIOSH.** Respirator Trusted-Source Information Page. *CDC.* [Online] February 22, 12. [Cited: August 9, 2012.] http://www.cdc.gov/niosh/npptl/topics/respirators/disp_part/RespSource3.html.